Quantitative histological correlates of NODDI orientation dispersion estimates in the human spinal cord

Francesco Grussu[1], Torben Schneider[1], Richard L. Yates[2], Mohamed Tachrount[3], Hui Zhang[4], Daniel C. Alexander[4], Gabriele C. DeLuca[2], and Claudia A. M. Wheeler-Kingshott[1]

[1]NMR Research Unit, Department of Neuroinflammation, Queen Square MS Centre, UCL Institute of Neurology, London, England, United Kingdom, [2]Nuffield Department of Clinical Neurosciences, University of Oxford, Oxford, England, United Kingdom, [3]Department of Brain Repair and Rehabilitation, UCL Institute of Neurology, London, England, United Kingdom, [4]Department of Computer Science and Centre for Medical Image Computing, University College London, London, England, United Kingdom

TARGET AUDIENCE Scientists interested in the quantification of central nervous system microstructure.

PURPOSE It has been shown that neurite orientation dispersion is an important feature at the MRI voxel scale even in organised areas such as the human corpus callosum[1,2]. Recently, it was also found to be a source of contrast between spinal cord grey and white matter (GM/WM)[3]. Here, we investigated for the first time the histological correlates of MRI-derived orientation dispersion estimates in a specimen of non-pathological human spinal cord. We employed neurite orientation dispersion and density imaging[4] (NODDI) to evaluate the orientation dispersion index (ODI), and compared it to structure tensor[5] (ST) metrics from sections of the same sample stained for axons and matching the radiographic fields of interest.

METHODS *MRI acquisition* One formalin-fixed specimen of human upper thoracic spinal cord was sectioned along the mid-sagittal plane in two parts, immersed in 10 mM phosphate buffered saline solution and scanned on a 9.4 T Agilent system at 35°C. A PGSE sequence was employed (TE/TR = 39.5/2200 ms; δ/Δ = 12/18 ms) to acquire twenty slices, 0.8 mm thick, parallel to the sectioning surface, with resolution of 0.164×0.200 mm^2 and field-of-view of 21×51.2 mm^2. Six diffusion-weighted (DW) shells were acquired with b = {520, 2080, 4680, 8320, 13000, 18720} s mm^{-2} and respectively {6, 15, 24, 33, 42, 51} directions, plus 25 non-DW images.

NODDI model fitting We fitted NODDI with the NODDI Matlab toolbox, after correcting b-values and gradient directions to account for diffusion weighting due to imaging gradients. This provided a voxel-wise map of ODI, ranging from 0 for parallel neurites to 1 for randomly oriented neurites.

Histology Routine histological procedures were followed to obtain two 10 µm thick sections, which were stained for axons (Palmgren Silver staining). Digital images of the stained sections were acquired with an Aperio slide scanner (ScanScope AT Turbo) at a magnification of 400×, and downsampled for a final pixel dimension of 1.008×1.008 µm^2.

ST calculation ST analysis of the histological images was performed in Matlab to quantify the local orientation dispersion[1,6]. After manual removal of neuronal cell bodies and blood vessels, we calculated the pixel-wise ST and derived maps of local dominant orientation $\theta \in [0; \pi]$ and anisotropy index $AI \in [0; 1]$, as in other studies[1,6]. We then split the maps into patches matching the in-plane MRI voxel dimensions, and calculated the patch-wise mean AI and circular variance ($CV \in [0; 1]$), where a higher CV corresponds to increased spread of θ. For each patch, we calculated CV as $CV = 1 - \left| N^{-1} \sum_{n=1}^{N} \exp(j\,2\theta_n) \right|$, with N being the number of pixel considered for analysis in the patch. CV is monotonically related to the maximum-likelihood estimate of the concentration parameter of a 2D Watson distribution.

Image registration Non-linear registration was performed in Matlab to warp AI and CV to the MRI space. The warping transformations were estimated from a set of matching control points manually drawn on the downsampled silver stained images and on the mean b = 0 image of the slice within which the sections were cut.

Analysis We compared NODDI ODI to ST indices after averaging maps from the two cuts. We drew an ROI on the mean b = 0 image, containing a mixture of GM and WM tissue and excluding areas of distortions and reduced coil sensitivity. Two additional ROIs were also drawn to define areas purely contained within GM and WM. We then calculated mean and standard deviation of AI, CV and ODI within the GM-only and WM-only ROIs. Lastly, we computed Pearson's correlation coefficient r between AI, CV and ODI within the three ROIs.

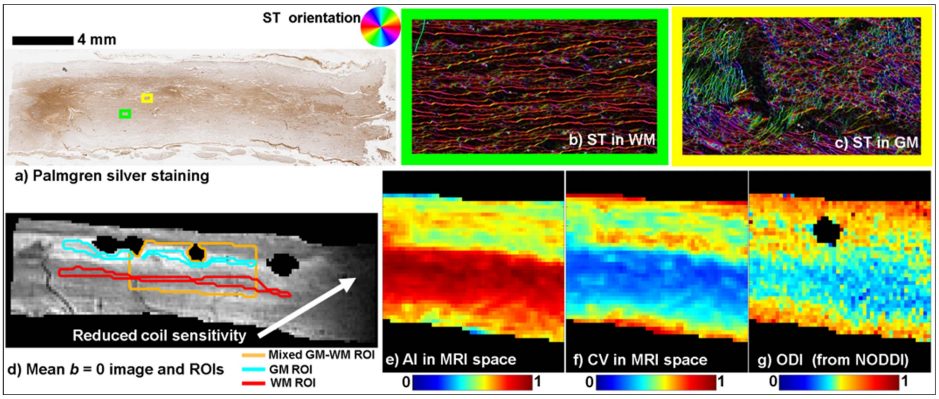

Figure 1: ST and NODDI analysis. a): silver stained image of one of the two cuts and position of boxes in b) and c). b)-c): ST in a WM and a GM area (orientation, AI and staining intensity encode Hue, Saturation and Value). d): mean b = 0 image and ROIs: GM in light blue, WM in red, mixed GM-WM ROI in orange. e)-g): particular of AI and CV warped to the MRI space and of ODI. Air bubbles were masked out in d) and g).

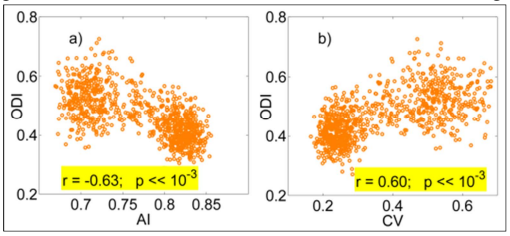

Figure 2: relation between NODDI ODI and ST AI and CV. a): scatter plot AI vs ODI for voxels within the orange ROI shown in figure 1.d). b): similar plot but for CV vs ODI. Pearson's correlation coefficients are highlighted in yellow.

RESULTS Figure 1 shows one of the silver stained images and corresponding ST and NODDI maps. Standard Hue-Saturation-Value (HSV) representation of the ST illustrates the complicated morphology of dendritic trees in GM, and highlights the presence of undulation and dispersion in WM. ST-derived parametric maps show that AI was higher in WM than in GM, whereas CV was higher in GM than in WM. NODDI ODI followed qualitatively the trend of CV. Means and standard deviations were AI = 0.72 ± 0.03, CV = 0.52 ± 0.10, ODI = 0.52 ± 0.06 in GM and AI = 0.81 ± 0.04, CV = 0.28 ± 0.10, ODI = 0.39 ± 0.05 in WM. Figure 2 illustrates voxel-by-voxel relation between ST indices and ODI, within the mixed GM-WM ROI. ODI was negatively correlated with AI and positively correlated with CV ($r = -0.63$ for AI; $r = 0.60$ for CV; $p \ll 0.001$). We also observed a significant correlation of ODI within the GM-only ROI ($r = -0.24$ for AI; $r = 0.22$ for CV; $p < 0.01$), whereas correlation within the WM-only ROI was found to be weak ($r = 0.10$, $p = 0.16$ for AI; $r = -0.17$, $p = 0.02$ for CV).

DISCUSSION AND CONCLUSION In this work, we have assessed the relationship between a DW-MRI derived neurite orientation dispersion metric (NODDI ODI), and its quantitative histological counterparts (ST AI and CV) in an *ex vivo* specimen of human spinal cord. ODI followed the same trend of ST indices, capturing the differences in terms of neurite morphology between GM and WM, and correlated with AI and CV within the ROI containing a mixture of the two tissue types. Although the contrast between GM and WM in both ODI and ST indices may have driven the observed correlation, we also measured a significant association within GM tissue. We observed a weaker correlation in WM, possibly because the range of orientation dispersion is narrower than in GM, and also because of the different thickness of the MRI slices compared to the stained sections. However, orientation dispersion was found to be non-negligible in WM given a mean CV of 0.28. This number corresponds to a full width at half maximum of a Watson distribution of roughly 45°, comparable to values reported in the human[1] and rat[7] corpus callosum. We conclude that NODDI accurately quantifies neurite orientation dispersion, which is a key microstructural feature of the human spinal cord at the MRI voxel scale.

ACKNOWLEDGEMENTS UK MS Society, EPSRC (EP/I027084/01, EP/G007748, EP/L022680/1), Department of Health's NIHR Biomedical Research Centres, UCL Grand Challenges, Oxford Brain Bank, the helpful work of all technicians (especially of J.C). The first and second listed authors are **joint first authors**; the last two listed authors are **joint senior authors**.

REFERENCES **1.** Budde MD, Annese J, Front Int Neurosc (2013); 7: 3. **2.** Ferizi U et al, Proc of MICCAI (2013); 8149, 74-81. **3.** Grussu F et al, Proc of ISMRM (2014); p.1720. **4.** Zhang H et al, NeuroImage (2012); 61(4): 1000-16. **5.** Bigün J, Granlund GH, Proc of 1st IEEE Int Conf on CV (1987); 433-38. **6.** Kleinnijenhuis M et al, Proc of OHBM (2013) **7.** Leergaard TB et al, PlosOne (2010); 5(1): e8595.